AIAA JOURNAL
Vol. 34, No. 2, February 1996

Skin-Friction Measurements and Calculations on a Lifting Airfoil

George G. Mateer* and Daryl J. Monson*
NASA Ames Research Center, Moffett Field, California 94035-1000
and
Florian R. Menter†
Eloret Institute, Sunnyvale, California 94035

A new technique for measuring skin friction was employed to help document the flow on an airfoil at angles of attack from −0.5 to 11.5 deg. Surface pressures were also measured on both the wing and wind-tunnel walls. The experiment was conducted at a freestream Mach number of 0.2 and Reynolds numbers of 0.6, 2, and 6 × 10^6. The objective of the study was to provide data and boundary condition information sufficient for the validation of numerical simulations. Such a simulation of the experiment was conducted using the INS2D Navier–Stokes code with the shear-stress-transport turbulence model. The computations provide a good description of both laminar and turbulent shear levels, except for turbulent flow on the top surface of the wing at the higher angles of attack.

Nomenclature

C_p = pressure coefficient
c = airfoil chord
c_f = skin-friction coefficient
H = shape factor
M = Mach number
n = index of refraction
q = dynamic pressure
R = constant in the oil density/temperature relationship
Re = freestream Reynolds number based on airfoil chord
S = constant in the oil viscosity/temperature relationship
s = airfoil span
T = temperature
t = time
U = axial velocity
x = axial coordinate from the wing leading edge
y = spanwise coordinate from the tunnel wall
z = vertical coordinate from the tunnel centerline
α = angle of attack
ζ = distance normal to model surface
θ = momentum thickness
θ_i = incidence angle
θ_r = refraction angle
λ = light wavelength
ξ = distance along model surface from oil leading edge
ρ = density
τ = skin friction
υ = viscosity

Subscripts

f = fringe
o = oil
ref = reference condition
run = tunnel run time
t = transition
∞ = free stream condition

Received April 25, 1995; presented as Paper 95-2192 at the AIAA 26th Fluid Dynamics Conference, San Diego, CA, June 19–22, 1995; revision received Sept. 14, 1995; accepted for publication Sept. 19, 1995.

*Research Engineer, Turbulence Physics and Modeling Branch, Aeronautical Technologies Division, M/S 229-1.
†Research Scientist. Member AIAA.

Introduction

THE use of high-pressure, blowdown facilities to simulate high Reynolds number flows has always been attractive because of the economies involved in smaller model construction. However, small scale makes it difficult to obtain skin friction in the attendant, thin boundary layers. Traditional methods[1] such as Preston tubes and pitot tube surveys are too intrusive for these flowfields, and floating element balances are too large to mount in the small models. A more recently developed method, the laser interferometer skin-friction (LISF) technique overcomes many of the limitations of the traditional methods. This approach utilizes lubrication theory to relate the local skin friction to the thinning of an oil film placed on the test surface. The film thickness is monitored by a laser beam photodiode interferometer. The technique provides a direct, nonintrusive measurement of skin friction that is relatively simple to use and may be applied in a wide variety of complex flows. Although several versions[2–6] of the method have been developed, some limitations remain. It is sensitive to possible dust contamination, tunnel vibration, model movement, and oil evaporation, and the procedure is very inefficient since only one measurement can be made per tunnel run.

Tanner and Blows[7] developed a photographic variant of the LISF technique to describe the thinning of the oil film. The oil was placed on a glass insert, and thinning was monitored by photographing the interference fringe pattern produced by illuminating the film with an He-Ne laser. The oil thickness was determined by measuring the fringe spacing from the photographs. This technique was neither convenient nor accurate, since it utilized a glass insert, manual fringe measurements, and crude estimates of effective tunnel run times. Thus it was eventually supplanted by the more convenient and accurate photodiode LISF method.

Recently, a modern extension and improvement on the original photographic LISF technique of Tanner and Blows has been developed. Termed the fringe-imaging skin-friction (FISF) method,[8] it is accurate and convenient to use and it doesn't require either a glass insert or a permanent installation in the test body. Also, it is insensitive to tunnel vibration, model movement, oil evaporation, and moderate dust contamination. Fringe imaging is carried out after a run with nonlaser light, so that tunnel optical access during a run is not required. Global skin-friction distributions can be obtained in a single run by using multiple drops or lines of oil.

The development of this measurement technique for skin friction provides new opportunities to do the detailed mapping of wall shear stresses necessary for the validation of numerical simulations. The present study is the first in a series of building block experiments designed to provide new, viscous information in increasingly complex

flows. A two-dimensional airfoil is used to provide the first, detailed, wall-shear distributions on both the upper and lower surfaces over a range of angles of attack. These data, when combined with pressure and boundary-layer transition measurements, will provide a baseline data set to establish a code's ability to simulate viscous flows.

Apparatus and Test Techniques

Facility

The investigation was conducted in the NASA Ames High Reynolds Channel No. II[9] (Fig. 1). This blowdown facility uses unheated dry air at ambient temperature. The high Reynolds number capability is achieved by testing at elevated total pressures (up to 7 atm). The test section is located inside a pressure shell that is maintained at essentially freestream static pressure by sidewall vent panels located just upstream from the diffuser. This technique alleviates many of the structural problems associated with high-pressure testing by reducing the pressure difference across the test section walls. The influence of the wind-tunnel walls on the flow is attenuated by 1) suction to reduce the sidewall boundary layers and 2) contouring the upper and lower walls. The present study utilized slightly divergent straight walls to account for boundary-layer growth.

As shown in Fig. 1 the stagnation chamber contains a number of screens to condition the flow by reducing the freestream turbulence level. The resulting rms fluctuation levels are 1) pressure = $0.02 \times q_\infty$ and 2) velocity = $0.005 \times U_\infty$.

Model and Test Conditions

The model (Fig. 2) used in this study was developed by Messerschmit-Bolkow-Blohm Transport-und Verkehrsflugzeuge of West Germany. It is a supercritical airfoil that combines high lift and low drag with moderate loading. Pressure taps were located primarily on the 50% span line with a lesser number at 25 and 75% span. The data were obtained at nominal freestream Mach numbers of 0.2 and angles of attack of −0.5, 3.5, 7.5, and 11.5 deg. The nominal angle of attack of the model was set relative to the wind-tunnel wall centerline to an accuracy of ±0.02 deg by rotating the model about its midchord. No stream angle measurements were made; consequently some uncertainty exists as to the actual value of angle of attack. The tests were carried out at Reynolds numbers of 0.6, 2, and 6×10^6 based on model chord. For this blowdown facility, the total temperature is a function of the run time. This variation was measured for each run with thermocouples located in the stagnation chamber.

To obtain skin-friction data the model was covered with a 2-mil Mylar® film that had an average surface roughness of 0.9μ.

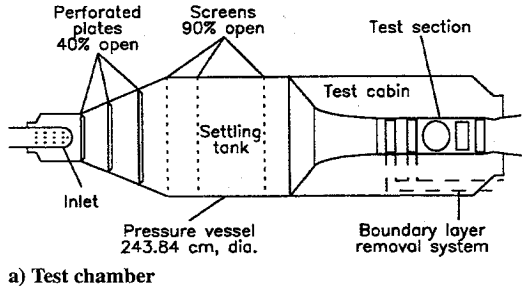

a) Test chamber

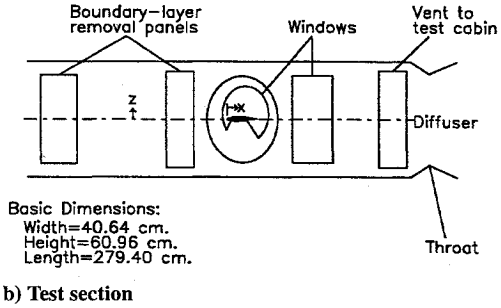

b) Test section

Fig. 1 NASA Ames high Reynolds number channel II.

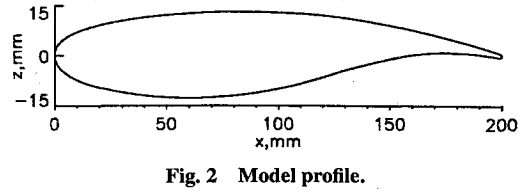

Fig. 2 Model profile.

Instrumentation

Pressure

Wall static pressures were measured on both the wing and wind-tunnel walls. All four tunnel walls were documented to provide boundary conditions for numerical simulations. Centerline pressures were measured on all walls from four chord lengths upstream to five downstream of the model leading edge. Sidewall pressures were also measured at $z/c = \pm 1.397$.

The static and total pressures used to determine the freestream Mach numbers were measured with Datametrics, Inc., model 570D transducers and model 1015 signal conditioners. These systems were calibrated at intervals during the test with a Consolidated Electrodynamics Corp., type 6-201-001 primary pressure standard. Calibrations were done over three separate ranges (0–0.68, 0–3.06, and 0–6.8 atm) for improved system accuracy. Based on these procedures and the specifications of the manufacturer, the overall system accuracy was estimated to be ±0.06% of reading. This translates to an uncertainty in Mach number of ±0.001. The remaining wall and wing pressures were measured with Pressure Systems, Inc., ESP-32 modules having ranges of ±0.34 and ±1.02 atm. These modules were mounted on constant temperature heaters to minimize temperature sensitivity of the calibrations. All modules were calibrated before each run over reduced ranges to minimize the uncertainty in the measurement. As a result of these measures, the static error band was reduced to approximately ±0.08% of full-scale reading and the corresponding uncertainty in pressure coefficient was ±0.002.

Shear

This study utilizes a new and innovative testing technique[8] to measure boundary-layer transition and global skin friction on wind-tunnel models. The FISF technique is a modern extension and improvement on the original photographic variant of the LISF technique of Tanner and Blows.[7] The basis of the method is in the principles of lubrication theory that relate the slope of the surface of a very thin layer of oil to the shear stress acting on it. The procedure, summarized in Fig. 3, consists of placing a drop or line of oil on a specularly reflecting surface and subjecting it to an airflow. The oil will be blown downstream, forming an inclined surface whose profile can be determined using interferometry.

By illuminating the oil with monochromatic light, interference fringes are produced due to the reflected light from the model surface interfering with that reflected from the oil surface. The inclination of the oil film can be determined by measuring the spacing between the fringes.

The relationship between skin-friction coefficient and fringe spacing was expressed in Ref. 8 as

$$c_f = \left[\frac{2(n_0\rho_0\nu_0)\,(\cos\theta_r)/(\cos\theta_i)}{q_\infty \lambda t_{\text{run}}}\right]\Delta\xi_f \qquad (1)$$

where the oil properties and the dynamic pressure are constant. In the present study these properties are variable because 1) the total

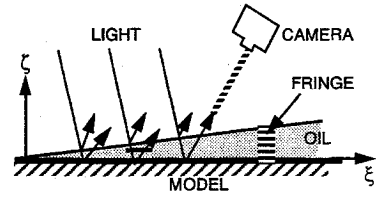

Fig. 3 Oil film interferometry.

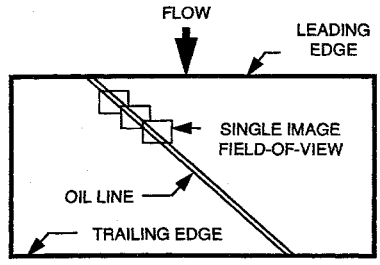

a) Wing planview; oil application

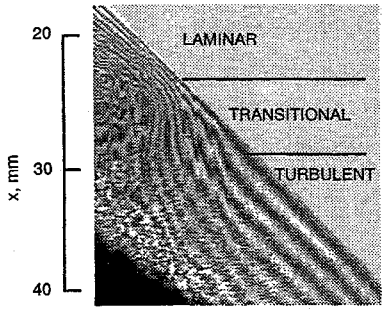

b) Typical oil fringe pattern

Fig. 4 Illustration of the FISF technique.

temperature varies with time and 2) q_∞ changes during the start up and shutdown of the tunnel. The oil viscosity and density were functions of model temperature as shown in the following equations:

$$\frac{\nu_0[T(t)]}{\nu_0(T_{\text{ref}})} = \exp\{-S[T(t) - T_{\text{ref}}]\} \tag{2}$$

$$\frac{\rho_0[T(t)]}{\rho_0(T_{\text{ref}})} = \exp\{-R[T(t) - T_{\text{ref}}]\} \tag{3}$$

The constants S and R are a function of the oil's nominal viscosity and density. The incident angle of the light was small so that $\cos\theta_r / \cos\theta_i \cong 1$. As a result of these considerations the equation for c_f becomes

$$c_f = \frac{2(n_0\rho_0\nu_0)_{\text{ref}} \times \Delta\xi_f}{\lambda \int_0^{t_{\text{run}}} q_\infty(t) \exp\{(S+R)[T(t) - T_{\text{ref}}]\}\, dt} \tag{4}$$

where the reference condition is $T_{\text{ref}} = 40°\text{C}$. Oil properties varied as follows: $1.399 \le n_0 \le 1.403$, $925 \le \rho_0 \le 957\ \text{kg/m}^3$, $10 \le \nu_0 \le 200$ cS, $0.0169 \le S \le 0.0178$ per °C, and $0.00108 \le R \le 0.00096$ per °C. Run times were typically 90 s and during that time the wall temperature would change by about 20°C. It is important to note that model wall temperature was measured independently and its time history differed from that of the tunnel's total temperature.

The limits of integration of Eq. (4) were determined experimentally by comparing data taken at the same angle of attack and Reynolds number but with different oil viscosities and run times. The most consistent values for c_f were obtained if time histories were integrated from the time the airflow started to when it stopped.

The application of the FISF technique to the present study is illustrated in Fig. 4. As described in Ref. 8, the model was first covered with an adhesive-backed Mylar film that improved the reflectivity at the oil/model interface, thereby enhancing the contrast between the light and dark fringes. A diagonal line of oil was placed across the model from the leading to trailing edges to provide a complete c_f distribution in one wind-tunnel run. This step represents a significant improvement in efficiency since approximately 3000 individual measurements of c_f could be made in a single run. A series of eight pictures were taken to completely document the fringe patterns over the entire chord. A typical image is shown in Fig. 4b where all three regions of boundary-layer flow (laminar, transitional, and turbulent) are clearly evident. Following a pair of adjacent fringes, laminar flow starts at the upper left of the picture and c_f decreases (fringes get closer together) as x increases (moving from left to right across the image). Transition is illustrated by the rapid increase in fringe spacing. Fringes are irregular in this region because of the spanwise variations in transition location. Transition is followed by fully turbulent fringes that are once again smooth and decrease in spacing with increasing x.

The spacing between fringes was measured by a computer. The images were digitized by a frame grabber connected to a 512×512 pixel, charge-coupled device (CCD) array, black and white video camera. After cropping the images to the start of the fringe patterns, low-pass digital filters were applied to the data in both the chord and spanwise directions to remove noise and small-scale anomalies. Minimums and maximums in the streamwise, intensity distributions were determined, and these pixel locations were then scaled to the model. Scaling was accomplished by photographing a ruler placed in the flow direction at the edge of each image. The first two fringes were typically used to determine the spacing.

The accuracy of the FISF method is discussed in detail in Ref. 8. To summarize, there are two major sources of error in determining c_f: 1) integrating the time histories of dynamic pressure and oil properties and 2) measuring the fringe spacing. Data taken at a constant angle of attack and Reynolds number but for a variety of oil viscosities and run times were used in conjunction with laminar c_f calculations to provide estimates of ±5% for the uncertainties in the integration. The factors affecting the accuracy of the fringe spacing measurement are much harder to quantify since they can change between images and within an image itself. For example, the image quality and resolution are two such factors. In an effort to quantify the uncertainty and yet account for its variability, the following technique was employed. Each image was treated separately by curvefitting the fringe spacing data and discarding any measurement that was greater than two standard deviations from the curvefit. The resulting uncertainty in the fringe spacing was approximately ±5%, and the overall uncertainty in the skin-friction coefficient is about ±7%.

Numerical Simulation

The mean flow solver in this study is the INS2D Navier–Stokes code developed at NASA Ames[10] combined with the shear-stress-transport (SST) turbulence model of Menter.[11] The SST model has produced very accurate results for a large number of aerodynamic flows and was therefore considered an ideal candidate for this comparison. A grid refinement study was performed to ensure that the solutions are grid independent. The following results have been computed on a 521×121 grid and only small differences were observed when compared with a 321×91 grid. By comparing free-air results with computations that included the tunnel walls, the influence of the walls on the pressure distribution was found to be negligible. To account for the walls a two grid Chimera scheme was utilized.

The transition model tested in this study was developed by Drela and Giles[12] and has been applied by various engineering groups.[13,14] It is based on the e^n model of Smith and Gamberoni[15] that assumes that transition occurs if the most unstable Tollmien–Schlichting wave has grown by a factor of e^n, with $n \sim 9$. The original e^n method requires a local stability analysis of the laminar boundary layer at every streamwise station and carries a high computational cost. Drela and Giles[12] have simplified the method considerably by correlating the growth of the disturbances to the integral properties of the boundary layer. The result is a single ordinary differential equation for the amplification rate n as a function of boundary-layer momentum thickness θ and the shape factor H.

Drela and Giles[12] developed their model in a framework where an integral boundary-layer code is strongly coupled to the inviscid Euler solver. The input for the stability equations comes from the integral boundary-layer code. More recently their stability analysis has also been incorporated into Navier–Stokes computations.[13]

When solving the Navier–Stokes equations, the integral boundary-layer properties can in theory be obtained from the solution[14]; however, this approach involves two major considerations. The first is the definition of a boundary-layer thickness, which is not easily obtained from the velocity profiles, especially during the early stages of the convergence process. The second is that laminar profiles are available only up to the transition location of the

last time iteration. If the transition location moves downstream during convergence, an extrapolation of the n factor into the turbulent region has to be performed. Both problems can be overcome, but the experience of the present authors is that the resulting code is not numerically robust.

Therefore, the input to the stability calculation was obtained from the solution of laminar integral boundary-layer equations, as in Ref. 13. This approach avoids both of the aforementioned problems and is computationally inexpensive. The only disadvantage is that the boundary-layer equations cannot be integrated past separation, since they are not strongly coupled to the Navier–Stokes solution and are singular at separation. Transition is therefore predicted at the location where n reaches a value of nine or where the boundary layer separates, whichever occurs first (see also Ref. 13). Note that boundary layers approaching separation have very high amplification rates, and transition in the experiment will generally be close to separation, especially for high Reynolds number flows.

Both the integral laminar boundary-layer equations and the simplified stability equations are taken exactly from Drela and Giles[12] and are therefore not repeated here. Transition in the SST model is achieved by setting the production term in the equation for the turbulent kinetic energy equal to zero upstream of the location where transition was determined by the stability analysis.

Results and Discussion

The initial part of this investigation was limited to defining the domain of two-dimensional flow. Both pressure and oilflow data were obtained for $\alpha \leq 20$ deg, and the results are summarized in the trailing-edge pressure distributions shown in Fig. 5.

For angles of attack greater than 11.5 deg asymmetric separation patterns developed on the wing upper surface as shown by the pressure distribution at $\alpha = 13.5$ deg. This observation was also substantiated by oilflow patterns that showed separation extending from the wing/wall junction to midspan. Consequently, angles of attack were limited to 11.5 deg or less to preserve the two-dimensionality of the cases included in the database.

A representative sample of the pressure data are shown in Fig. 6 for the angle-of-attack range. Although these results are for a Reynolds number of 2×10^6, similar results are available at the other Reynolds numbers; however, they are not shown because its effect was very small.

An important feature of these data is the effect of angle of attack on the inflection points in the pressure distributions. As will be shown later, the adverse pressure gradient has a strong effect on boundary-layer transition. On the upper surface the beginning of the adverse pressure gradient is very close to the leading edge, and although not obvious in the figure, it moves even closer as the angle of attack is increased. Also, the magnitude of the adverse pressure gradient increases significantly with angle of attack.

On the bottom surface these effects are just the opposite. As the angle of attack increases, the inflection point moves towards the trailing edge and the adverse pressure gradient decreases.

The experimental-computational comparisons of the pressure distributions are quite good over the angle-of-attack range. However, a full evaluation of a simulation must include comparisons with viscous data. The corresponding skin-friction distributions are shown on Fig. 7. The comparisons between simulation and experiment are quite good in the laminar region, thereby validating the FISF technique.

Computed levels of c_f in the turbulent region agree very well with the experiment on the bottom of the wing. However, they are overestimated on the top surface, particularly for the higher angles of attack. This might be expected at $\alpha = -0.5$ deg since there is such a large difference in transition location between the calculation and the experiment. For the higher α cases, however, transition is very close to the leading edge for both theory and experiment yet c_f is significantly overpredicted. Reasons for the discrepancies are unclear, but perhaps they are related to the very large pressure gradients on the top surface of the wing.

Boundary-layer transition points move forward on the top surface and rearward on the bottom surface as the angle of attack increases. A similar trend was noted in the location of the adverse pressure

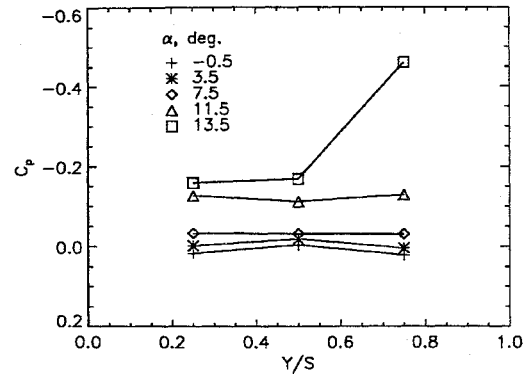

Fig. 5 Effect of α on the spanwise distribution of trailing-edge pressure; $Re = 2 \times 10^6$ and $M_\infty = 0.2$.

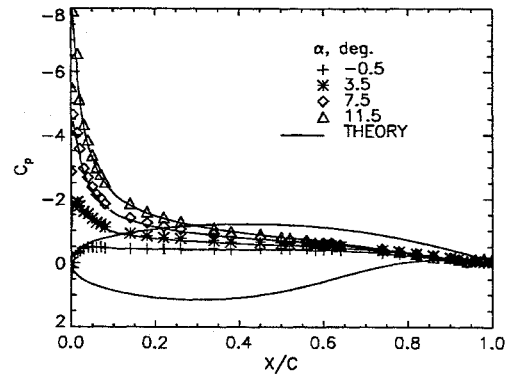

a) Top surface

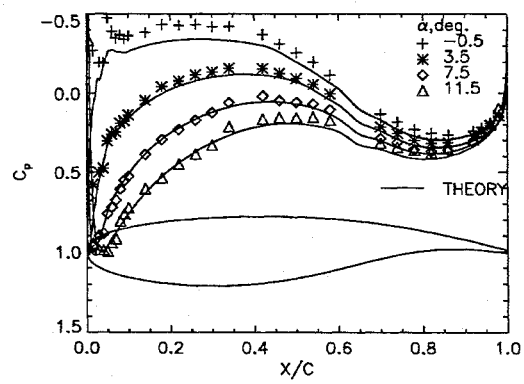

b) Bottom surface

Fig. 6 Effect of angle of attack on wing pressures; $Re = 2 \times 10^6$ and $M_\infty = 0.2$.

gradients in the pressure data. The computations provide a reasonably good description of the transition process (e.g., where it begins and ends) except at $\alpha = -0.5$ deg. Here the beginning of transition is much farther forward than the predictions. In fact, transition, on the top surface, only occurs in the simulation because the flow starts to separate.

Additional data were taken at $\alpha = -0.5$ deg to evaluate the ability of the simulation to describe the effect of Reynolds number on the flow. Tests were conducted at 0.6, 2, and 6×10^6 and the results are summarized in Fig. 8. At Reynolds numbers of 0.6 and 2×10^6 transition occurred prematurely in the calculation because the flow separated on the top surface. The comparisons show that for the top surface of the wing the experimental transition points are significantly upstream from those of the simulation. Transition Reynolds numbers based on θ are approximately 1×10^3 and 5×10^2 for the calculation and experiment, respectively. Transition on the upper surface responds primarily to Reynolds number changes since the pressure gradients are very small. On the bottom surface pressure gradient defines the theoretical location ($x/c \cong 0.45$), and the

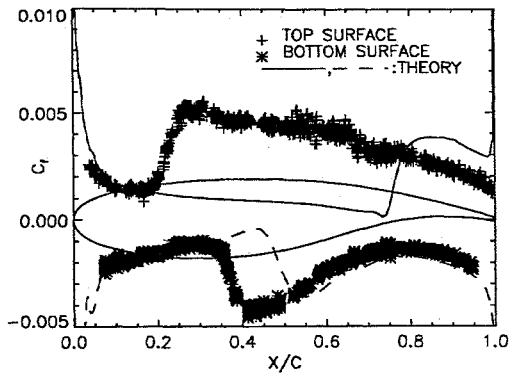

a) $\alpha = -0.5$ deg

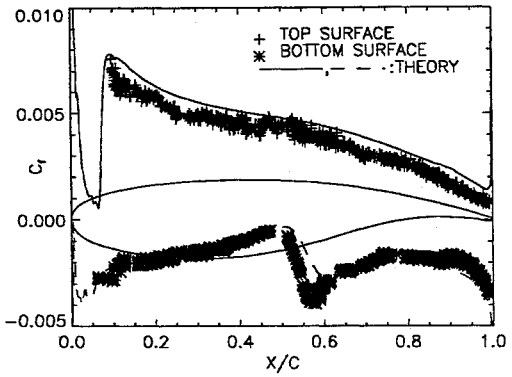

b) $\alpha = 3.5$ deg

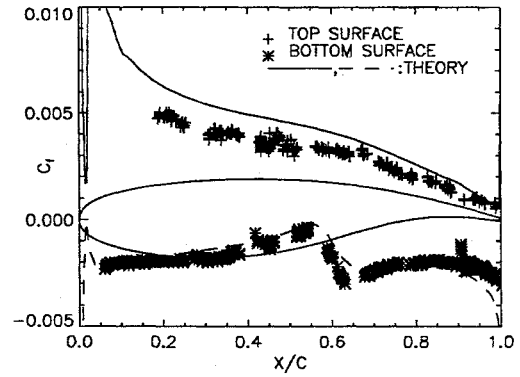

c) $\alpha = 7.5$ deg

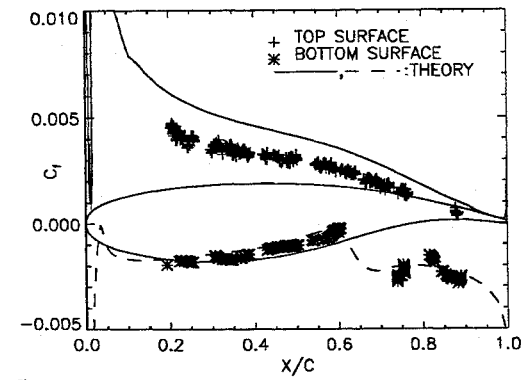

d) $\alpha = 11.5$ deg

Fig. 7 Effect of angle of attack on wing skin friction; $Re = 2 \times 10^6$ and $M_\infty = 0.2$.

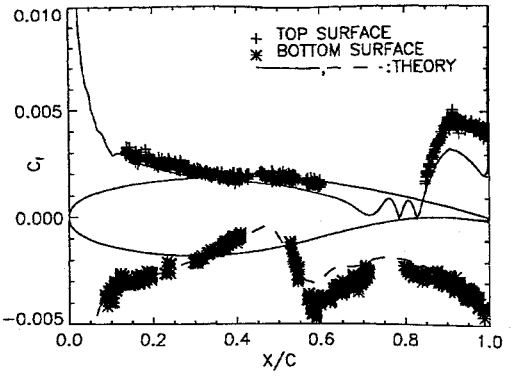

a) $Re = 0.6 \times 10^6$

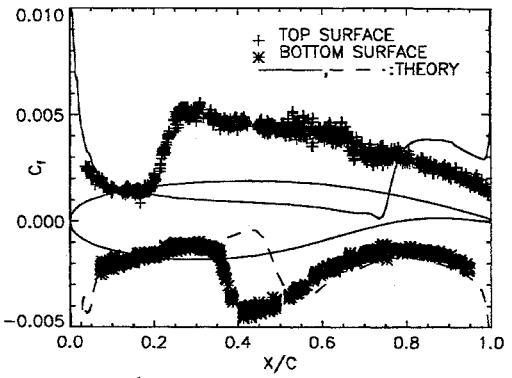

b) $Re = 2 \times 10^6$

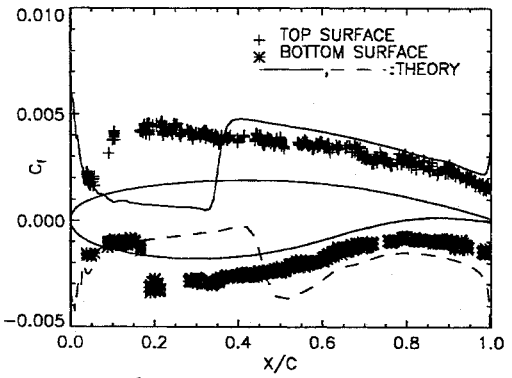

c) $Re = 6 \times 10^6$

Fig. 8 Effect of Reynolds number on wing skin friction; $\alpha = -0.5$ deg and $M_\infty = 0.2$.

combination (Reynolds number and pressure gradient) determines the experimental value. For $Re = 0.6 \times 10^6$ the pressure gradient fixes transition, whereas at the higher Reynolds numbers the location depends on the value of the Reynolds number. The inability of the simulation to describe the effect of Reynolds number on transition is due to the fact that transition takes place at much lower Reynolds numbers in the experiment. When the adverse pressure gradient is the root cause of transition, the calculation provides a very good indication of where it will occur.

A summary of boundary-layer transition results is presented in Fig. 9. Most of the experimental data points are average values for several runs. In Fig. 9a no data are shown for $\alpha > 3.5$ deg because transition was too far forward to accurately measure with FISF method. Also a limited amount of data were taken at intermediate Reynolds number to clarify the movement of transition. At $\alpha = -0.5$ deg on the upper surface these data support the observation that transition is essentially a function of the unit Reynolds number, i.e., $Re \times (x_t/c) = \text{const}$. At the higher angles of attack the adverse pressure gradients are so large near the nose that they determine the location of transition.

On the bottom surface, Fig. 9b, as the angle of attack increases, the local momentum thickness Reynolds numbers decrease so that adverse pressure gradients become more effective in determining transition locations. The computed transition locations are essentially independent of unit Reynolds number, a consequence of the large value of momentum thickness Reynolds number required for transition.

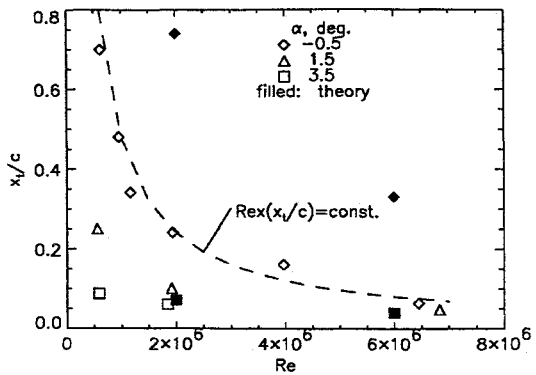

a) Top surface

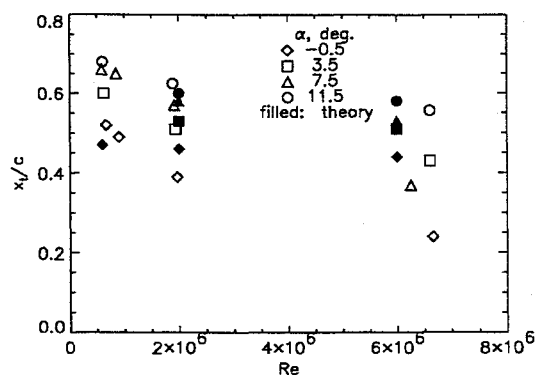

b) Bottom surface

Fig. 9 Measured and computed transition locations on wing.

Conclusions

Wall shear and pressure measurements have been obtained on a two-dimensional airfoil at $M_\infty = 0.2$ for a range of Reynolds numbers (0.6–6×10^6) and angles of attack (-0.5–11.5) deg. These data cover a wide range of laminar and turbulent shear stresses and provide a complete description of the effects of Reynolds number and pressure gradient on boundary-layer transition. A numerical simulation of the experimental data shows very good agreement with the pressure data. Laminar shear levels are calculated very well, but turbulent values are consistently overpredicted, particularly at the higher angles of attack. The location of boundary-layer transition is in good agreement with the computation when adverse pressure gradient is the root cause of transition. However, in the absence of strong gradients experimental, transition Reynolds numbers are less than half the theoretical value.

References

[1]Winter, K. G., "An Outline of the Techniques for the Measurement of Skin Friction in Turbulent Boundary Layers," *Progress in Aerospace Sciences*, Vol. 18, Pergamon, Oxford, England, UK, 1977, pp. 1–57.

[2]Tanner, L. H., "A Skin Friction Meter, Using the Viscosity Balance Principle, Suitable for Use with Flat or Curved Metal Surfaces," *Journal of Physics E: Scientific Instruments*, Vol. 10, No. 3, 1977, pp. 278–284.

[3]Monson, D. J., "A Nonintrusive Laser Interferometer Method for Measurement of Skin Friction," *Experiments in Fluids*, Vol. 1, No. 1, 1983, pp. 15–22.

[4]Westphal, R. V., Bachalo, W. D., and Houser, M. H., "Improved Skin Friction Meter," NASA TM 88216, March 1986.

[5]Kim, K. S., and Settles, G. S., "Skin-Friction Measurements by Interferometry," AGARDograph 315, May 1989, pp. 4.1–4.8.

[6]Seto, J., and Hornung, K., "Two-Directional Skin Friction Measurement Utilizing a Compact Internally-Mounted Thin-Liquid-Film Skin Friction Meter," AIAA Paper 93-0180, Jan. 1993.

[7]Tanner, L. H., and Blows, L. G., "A Study of the Motion of Oil Films on Surfaces in Air Flows, with Application to the Measurement of Skin Friction," *Journal of Physics E: Scientific Instruments*, Vol. 9, No. 3, 1976, pp. 194–202.

[8]Monson, D. J., Mateer, G. G., and Menter, F. R., "Boundary-Layer Transition and Global Skin Friction Measurement with an Oil-Fringe Imaging Technique," Society of Automotive Engineers, SAE Paper 932550, Warrendale, PA, Sept. 1993.

[9]McDevitt, J. B., Polek, T. E., and Hand, L. A., "A New Facility and Technique for Two-Dimensional Aerodynamic Testing," *Journal of Aircraft*, Vol. 20, No. 6, 1983, pp. 543–551.

[10]Rogers, S. E., and Kwak, D., "An Upwind Difference Scheme for the Time-Accurate Incompressible Navier–Stokes Equations," AIAA Paper 88-2583, June 1988; see also *AIAA Journal*, Vol. 28, No. 2, 1990, pp. 253–262.

[11]Menter, F. R., "Two-Equation Eddy-Viscosity Turbulence Models for Engineering Applications," *AIAA Journal*, Vol. 32, No. 8, 1994, pp. 1598–1605.

[12]Drela, M., and Giles, B. G., "Viscous-Inviscid Analysis of Transonic and Low Reynolds Number Airfoils," *AIAA Journal*, Vol. 25, No. 10, 1987, pp. 1347–1355.

[13]Kusunose, K., and Hoa, V. C., "Prediction of Transition Location for a 2-D Navier–Stokes Solver for Multi-Element Airfoil Configurations," AIAA Paper 94-2376, June 1994.

[14]Schneider, J., and Ewald, B., "Integration of Linear Stability Methods into Navier–Stokes Solvers for Computation of Transonic Laminar Airfoils," AIAA Paper 94-1849, June 1994.

[15]Smith, A. M. O., and Gamberoni, N., "Transition, Pressure Gradient, and Stability Theory," Douglas Aircraft Co., Rept. ES 26388, El Segundo, CA, Aug. 1956.